Letter

Instability of mixing layers: Momentum and thermal transport in the continuum breakdown regime

Vishnu Mohan [*]
School of Engineering, Newcastle University, Newcastle-upon-Tyne NE1 7RU, United Kingdom

A. Sameen
Department of Aerospace Engineering, Indian Institute of Technology Madras, Chennai 600036, India

Balaji Srinivasan
Department of Mechanical Engineering, Indian Institute of Technology Madras, Chennai 600036, India

Sharath S. Girimaji
Department of Ocean Engineering, Texas A&M University, College Station, Texas 77843, USA

We examine the momentum and thermal transport in the continuum breakdown regime of a mixing layer flow, which exhibits Kelvin-Helmholtz instability under ideal continuum conditions. The Grad 13 moment model is used as it provides an adequate description of the flow physics (second-order accurate in Knudsen number) in the transition regime. Analytical solutions are developed under breakdown conditions for two-dimensional, compressible, parallel shear flows. It is shown that the deviation of viscous stress and heat flux from the Navier-Stokes-Fourier system follows two different scaling regimes depending upon the Mach number. At low Mach numbers, the departure of all stress and heat-flux components depends only upon the Knudsen number. At high Mach number, the scaling of shear stress and transverse heat flux depends on the product of the Knudsen and Mach numbers. The normal stresses depend individually on the Knudsen and Mach number. The scaling results are verified against numerical simulations of compressible mixing layers performed using the unified gas kinetic scheme for various degrees of rarefaction.

Introduction. Rarefaction effects are important in many flows encountered in nature and engineering applications—including astrophysical flows, space propulsion, re-entry flight, high-altitude vehicles, and micro-electro-mechanical (MEMS) systems. For highly rarefied flows, the foundational Boltzmann equation can be solved using the direct simulation Monte Carlo (DSMC) approach or discrete velocity methods (DVM) at reasonable computational cost. In space applications such as satellite thruster flow, multiple levels of rarefaction flow—from a continuum to free-molecular regime—are present within a single application [1–4]. A possible simulation approach would be to employ separate physical models in different rarefaction regimes. In this regard, it is of much importance to understand the conditions under which mass, momentum, and thermal transport depart from the continuum Navier-Stokes-Fourier (NSF) system of equations. It is also of fundamental interest to examine the

manner of continuum breakdown in different regimes of Mach number.

Kelvin-Helmholtz instability (KHI) occurs at the interface of fast and slow moving streams under favorable conditions. Such flows are called mixing layers and the onset of KHI at high enough Reynolds numbers enhances the mixing of momentum and energy between the two streams [5]. In a variety of aerospace propulsion and astrophysical mixing layer flows, the standard KHI is profoundly influenced by compressibility and rarefaction effects [6–10]. In our recent work [11], the unified gas kinetic scheme (UGKS) simulations were used to establish that mixing layers exhibit five types of behavior in the parameter space of Mach (Ma) and Knudsen (Kn) numbers. At low Ma and Kn, the well-known KHI is observed. The flow physics in this regime is well understood. When Ma is increased at low Kn, the emergence of a dilatational velocity field leads to the inhibition of KHI and reduced mixing. At low Ma and high Kn, the mixing layer diffuses rapidly without the occurrence of KHI. This is because molecules translate freely from one side of the mixing layer to the other without encountering many collisions. In the fourth regime of high Kn and Ma, a combination of dilatational waves and free-molecular translation leads to a more restrained mixing, again without the occurrence of KHI. The purpose of the study is to examine the continuum breakdown regime which separates the

---

*Corresponding author: vishnu.mohan@newcastle.ac.uk

TABLE I. Various continuum breakdown parameters proposed in the literature.

	Reference	Breakdown parameters	Remarks
Macroscopic parameter	Tsien [13]	$(\gamma - 1)\text{Ma}^2/\text{Re}$	$\text{Re} \approx \text{Ma}/\text{Kn} \Rightarrow \text{Ma}^2/\text{Re} \approx$ MaKn, MaKn is the ratio of micro to macro timescale.
	Bird [14]	$P = \lambda \frac{D(\ln\rho)}{Dt}$	Empirical formulation, fails at low Mach.
	Boyd *et al.* [15]	$\text{Kn}_{GLL} = \frac{\lambda}{Q}|\nabla Q|$	Q is either T or ρ, local parameter.
	Schrock *et al.* [16,17]	$\mathscr{W} = \frac{\partial \rho s}{\partial t} + \nabla \cdot \vec{\mathscr{T}}$	$\mathscr{W}$ is entropy generation rate, s is entropy per mass, $\mathscr{T}$ is entropy flux. Method was used for DSMC.
	Lockerby *et al.* [18]	$\text{Kn}_Q = \frac{\|Q - Q^{NS}\|}{\|Q^{NS}\|}$	Q can be σ_{ij} and q_i, $\|\cdot\|$ is L_2 norm over the components, $\|Q^{NS}\|$ should be nonzero.
	Mohan *et al.* [12]	$\text{Kn}_g = \frac{\partial}{\partial y}\left(\frac{\lambda u}{a}\right)$	Local continuum breakdown parameter based on KnMa.
PDF parameter	Chigullapalli *et al.* [19]	$\dot{S}_{coll} = -\nu \int_{-\infty}^{\infty}(f - f_0)\ln\left(\frac{h^3 f}{m^3}\right)d\vec{c}$	Method used in DVM solver. Used to test accuracy of scheme and grid.
	Meng *et al.* [20]	$E_c^{NS} = \sqrt{\frac{\int(f - f^{NS} - f^0)^2 d\vec{c}}{\int(f^2)d\vec{c}}}$	*A priori* prediction difficult for NSF to Boltzmann switch;
	Alamatsaz and Venkattraman [21]	$\epsilon = \frac{\int|\phi - \phi_{CE}|d\vec{\omega}}{\int|\phi_{CE}|d\vec{\omega}}$	ϕ is Fourier transform of f.

parameter region of KHI occurrence from the dominantly diffusive behavior. Mohan *et al.* [12] demonstrates that in a high-speed rarefied mixing layer, the onset of Navier-Stokes continuum breakdown effects is different for shear and normal stresses. Similarly, the breakdown of transverse and normal heat fluxes exhibits markedly different features. Current breakdown criteria treat all flux and stress components in an identical fashion and do not adequately account for directional effects. It is important to note that many of the flows of practical importance are shear flows.

The various parameters developed in the literature to characterize the continuum breakdown in rarefied compressible flows are listed in Table I. The different approaches can be classified into two categories: (i) macroscopic or continuum field based parameters and (ii) kinetic theory or the particle distribution function (PDF) based parameters. Expressions similar to the ones listed in Table I have also been suggested by Singh and Schwartzentruber [2], Tiwari [22], Ou and Chen [23], Singh and Schwartzentruber [3], Wang *et al.* [4], and Macrossan [24]. The methods used in the literature, while useful, do not provide a complete account of all breakdown scenarios.

The objective of this work is to use the Grad 13 moment model to analytically characterize the continuum breakdown and identify the difference in the breakdown between the normal and shear or transverse transport. It is well established in the literature that the Grad's moment equations are not completely valid for high Knudsen numbers; for example, they fail to describe smooth shock structures for Mach numbers above a critical value [25]. However, the model is quite suitable for up to second-order expansion in the Knudsen number. Since continuum breakdown phenomena only address the limits of first-order expansion, it is reasonable to use the Grad 13 model for this purpose.

Grad 13 moment equations. The Boltzmann transport equation provides an accurate description of the evolution of the single-point PDF over a wide range of Knudsen and Mach numbers. The NSF [26], Grad 13 moment [27], and Regularized 13 moment equations [28,29], which provide macroscopic descriptions of the medium, are obtained by taking the moments of the Boltzmann equation. The NSF equation uses an algebraic relationship for the description of stress and heat flux and is accurate up to $O(\text{Kn})$. The Grad 13 moment equation is accurate up to $O(\text{Kn}^2)$ and the Regularized 13 moment equation is accurate up to $O(\text{Kn}^3)$. The 13-moment approaches entail transport equations for stress and heat flux. Here, the Grad 13 description is used since our concern is restricted to deviation from the NSF equation.

The macroscopic mass, momentum, and energy conservation equations for a monoatomic gas are given as [26]

$$\frac{D\rho}{Dt} + \rho \frac{\partial u_i}{\partial x_i} = 0, \tag{1}$$

$$\rho \frac{Du_i}{Dt} + \frac{\partial p}{\partial x_i} + \frac{\partial \tau_{ik}}{\partial x_k} = 0, \tag{2}$$

$$\frac{3}{2}\rho \frac{D\theta}{Dt} + \rho\theta \frac{\partial u_i}{\partial x_i} + \frac{\partial q_i}{\partial x_i} + \tau_{ij}\frac{\partial u_i}{\partial x_j} = 0, \tag{3}$$

where $D/Dt = \partial/\partial t + u_i \partial/\partial x_i$ is the material derivative, ρ is the density, p is the pressure, $\theta = RT$, where T is temperature, R is the gas constant, x_i are the Cartesian coordinates (x, y, z), u_i are velocity components, τ_{ij} are the stress components, and q_i are the heat flux components. Equations for the stress and

heat-flux components in a Grad 13 moment system for the Bhatnagar-Gross-Krook assumption [26] are given as

$$\frac{D\tau_{ij}}{Dt} + \frac{4}{5}\frac{\partial q_{<i}}{\partial x_{j>}} + 2\tau_{k<i}\frac{\partial u_{j>}}{\partial x_k} + \tau_{ij}\frac{\partial u_k}{\partial x_k} + 2p\frac{\partial u_{<i}}{\partial x_{j>}}$$
$$= -\frac{p}{\mu}\tau_{ij}, \tag{4}$$

$$\frac{Dq_i}{Dt} + \frac{5}{2}p\frac{\partial\theta}{\partial x_i} + \frac{5}{2}\tau_{ij}\frac{\partial\theta}{\partial x_j} - \tau_{ij}\theta\frac{\partial ln\rho}{\partial x_j} - \frac{\tau_{ij}}{\rho}\frac{\partial\tau_{jk}}{\partial x_k}$$
$$- \frac{5}{2}\theta\frac{\partial\tau_{ij}}{\partial x_j} + \theta\frac{\partial\tau_{ij}}{\partial x_j} + \frac{5}{7}q_i\frac{\partial u_j}{\partial x_j} + \frac{7}{5}q_j\frac{\partial u_i}{\partial x_j} + \frac{7}{5}q_j\frac{\partial u_j}{\partial x_i}$$
$$= -\frac{p}{\mu}q_i, \tag{5}$$

where $a_{<i}b_{j>} = (a_ib_j + a_jb_i)/2 - (1/3)a_ib_i\delta_{ij}$ is the traceless symmetric matrix, and μ is the dynamic viscosity. Clearly, the Grad 13 moment equation is quite complex for general flows. In order to obtain useful insights into shear flows of practical importance, the following approximations are made: (i) Nonparallel effects are neglected (i.e., $\partial/\partial x = 0$), (ii) spanwise velocity u_z is assumed to be zero, (iii) stress and heat flux in the spanwise direction (z) is negligible, (iv) the Chapman-Enskog relationship, $\nu = p/\mu$, is valid in the near-continuum limit [30], and (v) the continuum scalings of the flow variables are assumed to be valid in the near-continuum regime. It is important to note that the time derivatives can be nonzero.

The above assumptions reduce mass, momenta in the x and y directions, and energy equations as follows:

$$\frac{\partial\rho}{\partial t} + \frac{\partial\rho u_y}{\partial y} = 0, \tag{6}$$

$$\rho\frac{\partial u_x}{\partial t} + \rho u_y\frac{\partial u_x}{\partial y} + \frac{\partial\tau_{xy}}{\partial y} = 0, \tag{7}$$

$$\rho\frac{\partial u_y}{\partial t} + \rho u_y\frac{\partial u_y}{\partial y} + \frac{\partial\tau_{yy}}{\partial y} + \frac{\partial p}{\partial y} = 0, \tag{8}$$

$$\frac{3}{2}\rho\frac{\partial\theta}{\partial t} + \frac{3}{2}\rho u_y\frac{\partial\theta}{\partial y} + p\frac{\partial u_y}{\partial y} + \frac{\partial q_y}{\partial y} + \tau_{xy}\frac{\partial u_x}{\partial y} + \tau_{yy}\frac{\partial u_y}{\partial y}$$
$$= 0. \tag{9}$$

The stress (τ_{xy}, τ_{yy}, and τ_{xx}) and heat flux (q_y and q_x) component equations reduce to

$$\tau_{xy} = -\mu\frac{\partial u_x}{\partial y} - \frac{1}{\nu}\left[\frac{\partial}{\partial t}(\tau_{xy}) + \frac{\partial}{\partial y}(u_y\tau_{xy}) + \frac{2}{5}\frac{\partial}{\partial y}(q_x) + \tau_{yy}\frac{\partial}{\partial y}(u_x) + \tau_{xy}\frac{\partial}{\partial y}(u_y)\right], \tag{10}$$

$$\tau_{yy} = -\frac{4}{3}\mu\frac{\partial u_y}{\partial y} - \frac{1}{\nu}\left[\frac{\partial}{\partial t}(\tau_{yy}) + u_y\frac{\partial}{\partial y}(\tau_{yy}) + \frac{8}{15}\frac{\partial}{\partial y}(q_y) + \frac{7}{3}\tau_{yy}\frac{\partial}{\partial y}(u_y) - \frac{2}{3}\tau_{xy}\frac{\partial}{\partial y}(u_x)\right], \tag{11}$$

$$\tau_{xx} = \frac{2}{3}\mu\frac{\partial u_y}{\partial y} - \frac{1}{\nu}\left[\frac{\partial\tau_{xx}}{\partial t} + u_y\frac{\partial\tau_{xx}}{\partial y} + \tau_{xx}\frac{\partial u_y}{\partial y} - \frac{4}{15}\frac{\partial q_y}{\partial y} + \frac{4}{3}\tau_{xy}\frac{\partial u_x}{\partial y} - \frac{2}{3}\tau_{yy}\frac{\partial u_y}{\partial y}\right], \tag{12}$$

$$q_x = -\frac{1}{\nu}\left[\frac{\partial}{\partial t}(q_x) + u_y\frac{\partial}{\partial y}(q_x) + \frac{5}{2}\tau_{xy}\frac{\partial}{\partial y}(\theta) - \tau_{xy}\theta\frac{\partial}{\partial y}(ln\rho) - \frac{\tau_{xx}}{\rho}\frac{\partial}{\partial y}(\tau_{xy}) - \frac{\tau_{xy}}{\rho}\frac{\partial}{\partial y}(\tau_{yy}) + \theta\frac{\partial}{\partial y}(\tau_{xy}) + \frac{7}{5}q_y\frac{\partial}{\partial y}(u_x) + \frac{7}{5}q_x\frac{\partial}{\partial y}u_y\right], \tag{13}$$

$$q_y = -\frac{5\mu}{2}\frac{\partial\theta}{\partial y} - \frac{1}{\nu}\left[\frac{\partial}{\partial t}(q_y) + u_y\frac{\partial}{\partial y}(q_y) + \frac{5}{2}\tau_{yy}\frac{\partial}{\partial y}(\theta) - \tau_{yy}\theta\frac{\partial}{\partial y}(ln\rho) - \frac{\tau_{xy}}{\rho}\frac{\partial}{\partial y}(\tau_{xy}) - \frac{\tau_{yy}}{\rho}\frac{\partial}{\partial y}(\tau_{yy}) + \theta\frac{\partial}{\partial y}(\tau_{yy})\right.$$
$$\left. + \frac{16}{5}q_y\frac{\partial}{\partial y}(u_y) + \frac{2}{5}q_x\frac{\partial}{\partial y}u_x\right]. \tag{14}$$

The first terms on the right-hand side of Eqs. (10)–(14) are the NSF continuum stress tensor and heat-flux vector [30] constitutive relations. The terms in the square brackets correspond to the higher-order term.

The nondimensional parameters of importance in the present study are Reynolds number Re, Mach number Ma, and Knudsen number Kn, which are given as

$$\mathrm{Re} = \frac{\rho_\infty u_\infty \delta_0}{\mu_\infty}, \quad \mathrm{Ma} = \frac{u_\infty}{c_\infty}, \quad \mathrm{Kn} = \frac{\lambda}{\delta_0}. \tag{15}$$

Here, ρ_∞ is the free-stream density, u_∞ is the free-stream velocity, δ_0 is the shear layer thickness, μ_∞ is the free-stream dynamic viscosity, c_∞ is the free-stream speed of sound, and λ is the mean-free path of the medium. For monoatomic gas,

the specific heat capacity at constant pressure, $C_p = 5R/2$. It has been shown by Tsien [13] that Re $\approx$ Ma/Kn.

Nondimensionalization of equations. The temporal equivalent of the thin shear layer approximation in the continuum limit is invoked in nondimensionalizing the Grad 13 moment equation. The order analysis based on the thin shear layer assumption reasons that the diffusion layer thickness δ_0 develops through viscous action. The scales used for the nondimensionalization of the variables are shown in Table II. The collision frequency ν scales as λ/c_∞, which is the inverse of the molecular timescale. Using the Crocco-Busemann relationship [31] for the compressible boundary layer flow with zero streamwise pressure gradient, the temperature can be shown to be directly proportional to u_∞^2.

TABLE II. Nondimensionalization of different variables. The quantities with the overbar are nondimensional.

$\bar{y} = y/\delta_0$	$\bar{\rho} = \rho/\rho_\infty$
$\bar{\mu} = \mu/\mu_\infty$	$\bar{\tau}_{xy} = (\delta_0 \tau_{xy})/(\mu_\infty u_\infty)$
$\bar{u}_x = u_x/u_\infty$	$\bar{u}_y = (\rho_\infty \delta_0 u_y)/\mu_\infty$
$\bar{t} = (\mu_\infty t)/(\rho_\infty \delta_0^2)$	$\bar{p} = p/(\rho_\infty u_\infty^2)$
$\bar{\theta} = \theta/u_\infty^2$	$\bar{\nu} = \lambda \nu/c_\infty$
$\bar{\tau}_{yy} = (\rho_\infty \delta_0^2 \tau_{yy})/\mu_\infty^2$	$\bar{\tau}_{xx} = (\rho_\infty \delta_0^2 \tau_{xx})/\mu_\infty^2$
$\bar{q}_y = (\delta_0 q_y)/(\mu_\infty u_\infty^2)$	$\bar{q}_x = (c_\infty \delta_0^2 q_x)/(\mu_\infty u_\infty^3 \lambda)$

Substituting these nondimensionalized variables into Eqs. (7)–(9), we get

$$\frac{\mu_\infty}{\delta_0^2}\left\{ \frac{\partial \bar{\rho}}{\partial \bar{t}} + \frac{\partial \bar{\rho}\bar{u}_y}{\partial \bar{y}} \right\} = 0, \qquad (16)$$

$$\frac{\mu_\infty u_\infty}{\delta_0^2}\left\{ \bar{\rho}\frac{\partial \bar{u}_x}{\partial \bar{t}} + \bar{\rho}\bar{u}_y\frac{\partial \bar{u}_x}{\partial \bar{y}} + \frac{\partial \bar{\tau}_{xy}}{\partial \bar{y}} \right\} = 0, \qquad (17)$$

$$\frac{\rho_\infty u_\infty^2}{\delta_0}\left\{ \frac{1}{\mathrm{Re}^2}\left(\bar{\rho}\frac{\partial \bar{u}_y}{\partial \bar{t}} + \bar{\rho}\bar{u}_y\frac{\partial \bar{u}_y}{\partial \bar{y}} + \frac{\partial \bar{\tau}_{yy}}{\partial \bar{y}} \right) + \frac{\partial \bar{p}}{\partial \bar{y}} \right\} = 0, \quad (18)$$

$$\frac{\mu_\infty u_\infty^2}{\delta_0^2}\left\{ \frac{3}{2}\bar{\rho}\frac{\partial \bar{\theta}}{\partial \bar{t}} + \frac{3}{2}\bar{\rho}\bar{u}_y\frac{\partial \bar{\theta}}{\partial \bar{y}} + \bar{p}\frac{\partial \bar{u}_y}{\partial \bar{y}} + \frac{\partial \bar{q}_y}{\partial \bar{y}} + \bar{\tau}_{xy}\frac{\partial \bar{u}_x}{\partial \bar{y}} \right.$$
$$\left. + \frac{1}{\mathrm{Re}^2}\bar{\tau}_{yy}\frac{\partial \bar{u}_y}{\partial \bar{y}} \right\} = 0. \qquad (19)$$

Order of magnitude of stresses and heat fluxes. Nondimensionalizing the τ_{xy}, τ_{yy}, and τ_{xx} in Eqs. (10)–(12) as discussed above, and noting that the nondimensional frequency $\bar{\nu} = \lambda \nu/c_\infty$, by definition, is of the order of unity, we get

$$\frac{\delta_0 \tau_{xy}}{\mu_\infty u_\infty} = -\bar{\mu}\frac{\partial \bar{u}_x}{\partial \bar{y}} - \frac{1}{\bar{\nu}}\left[\mathrm{Kn}^2\left(\frac{\partial \bar{\tau}_{xy}}{\partial \bar{t}} + \frac{\partial \bar{u}_y \bar{\tau}_{xy}}{\partial \bar{y}} + \bar{\tau}_{xy}\frac{\partial \bar{u}_y}{\partial \bar{y}} + \bar{\tau}_{yy}\frac{\partial \bar{u}_x}{\partial \bar{y}} \right) + \frac{2\mathrm{Kn}^2\mathrm{Ma}^2}{5}\frac{\partial \bar{q}_x}{\partial \bar{y}} \right], \qquad (20)$$

$$\frac{\rho_\infty \delta_0^2 \tau_{yy}}{\mu_\infty^2} = -\frac{4}{3}\bar{\mu}\frac{\partial \bar{u}_y}{\partial \bar{y}} - \frac{1}{\bar{\nu}}\left[\mathrm{Kn}^2\left(\frac{\partial \bar{\tau}_{yy}}{\partial \bar{t}} + \bar{u}_y\frac{\partial \bar{\tau}_{yy}}{\partial \bar{y}} + \frac{7}{3}\bar{\tau}_{yy}\frac{\partial \bar{u}_y}{\partial \bar{y}} \right) + \mathrm{Ma}^2\left(\frac{8}{15}\frac{\partial \bar{q}_y}{\partial \bar{y}} - \frac{2}{3}\bar{\tau}_{xy}\frac{\partial \bar{u}_x}{\partial \bar{y}} \right) \right], \qquad (21)$$

$$\frac{\rho_\infty \delta_0^2 \tau_{xx}}{\mu_\infty^2} = \frac{2}{3}\bar{\mu}\frac{\partial \bar{u}_y}{\partial \bar{y}} - \frac{1}{\bar{\nu}}\left[\mathrm{Kn}^2\left(\frac{\partial \bar{\tau}_{xx}}{\partial \bar{t}} + \bar{u}_y\frac{\partial \bar{\tau}_{xx}}{\partial \bar{y}} + \bar{\tau}_{xx}\frac{\partial \bar{u}_y}{\partial \bar{y}} - \frac{2}{3}\bar{\tau}_{yy}\frac{\partial \bar{u}_y}{\partial \bar{y}} \right) + \mathrm{Ma}^2\left(\frac{4}{15}\frac{\partial \bar{q}_y}{\partial \bar{y}} + \bar{\tau}_{xy}\frac{\partial \bar{u}_x}{\partial \bar{y}} \right) \right]. \qquad (22)$$

The nondimensional equation for q_x and q_y from Eqs. (13) and (14) are given as

$$\frac{c_\infty \delta_0^2 q_x}{\mu_\infty u_\infty^3 \lambda} = -\frac{1}{\bar{\nu}}\left[\mathrm{Kn}^2\left(\frac{\partial \bar{q}_x}{\partial \bar{t}} + \bar{u}_y\frac{\partial \bar{q}_x}{\partial \bar{y}} + \frac{7}{5}\bar{q}_x\frac{\partial \bar{u}_y}{\partial \bar{y}} \right) - \frac{\mathrm{Kn}^2}{\mathrm{Ma}^2}\left(\frac{\bar{\tau}_{xy}}{\bar{\rho}}\frac{\partial \bar{\tau}_{yy}}{\partial \bar{y}} + \frac{\bar{\tau}_{xx}}{\bar{\rho}}\frac{\partial \bar{\tau}_{xy}}{\partial \bar{y}} \right) + \frac{5}{2}\bar{\tau}_{xy}\frac{\partial \bar{\theta}}{\partial \bar{y}} \right.$$
$$\left. - \bar{\tau}_{xy}\bar{\theta}\frac{\partial(\ln\bar{\rho})}{\partial \bar{y}} + \bar{\theta}\frac{\partial \bar{\tau}_{xy}}{\partial \bar{y}} + \frac{7}{5}\bar{q}_y\frac{\partial \bar{u}_x}{\partial \bar{y}} \right], \qquad (23)$$

$$\frac{\delta_0 q_y}{\mu_\infty u_\infty^2} = -\frac{5\bar{\mu}}{2}\frac{\partial \bar{\theta}}{\partial \bar{y}} - \frac{1}{\bar{\nu}}\left[-\frac{\mathrm{Kn}^4}{\mathrm{Ma}^2}\frac{\bar{\tau}_{xx}}{\bar{\rho}}\frac{\partial \bar{\tau}_{yy}}{\partial \bar{y}} + \frac{2\mathrm{Kn}^2\mathrm{Ma}^2}{5}\bar{q}_x\frac{\partial \bar{u}_x}{\partial \bar{y}} - \mathrm{Kn}^2\left(\frac{\partial \bar{q}_y}{\partial \bar{t}} + \bar{u}_y\frac{\partial \bar{q}_y}{\partial \bar{y}} + \frac{16}{5}\bar{q}_y\frac{\partial \bar{u}_y}{\partial \bar{y}} - \frac{\bar{\tau}_{xy}}{\bar{\rho}}\frac{\partial \bar{\tau}_{xy}}{\partial \bar{y}} + \frac{5}{2}\bar{\tau}_{yy}\frac{\partial \bar{\theta}}{\partial \bar{y}} \right.\right.$$
$$\left.\left. - \bar{\tau}_{yy}\bar{\theta}\frac{\partial(\ln\bar{\rho})}{\partial \bar{y}} + \bar{\theta}\frac{\partial \bar{\tau}_{yy}}{\partial \bar{y}} \right) \right]. \qquad (24)$$

At the continuum, only $O(\mathrm{Kn})$ terms are important; however, increasing the rarefaction $O(\mathrm{Kn}^2)$ terms determines the departure from the NSF equation. From Eqs. (20)–(24), the higher-order terms in the continuum breakdown mechanism can now be extracted. From the above equations, it can be seen that the leading-order terms in all of the above equations are the continuum terms. The next higher-order terms are as follows:

(1) for the transverse heat flux and shear stress, they are Kn^2 and $\mathrm{Kn}^2\mathrm{Ma}^2$;

(2) for the normal stress, they are Kn^2 and Ma^2.

When $\mathrm{KnMa} \ll \mathrm{Kn}$ (i.e., when $\mathrm{Ma} \ll 1$), the leading-order terms in the transverse heat flux and shear stress are the ones that have Kn^2 as the coefficient. This implies that for incompressible flows, the deviation of τ_{xy} and q_y from the NSF equation scales as Kn^2. When $\mathrm{KnMa} \gg \mathrm{Kn}$ (i.e., when $\mathrm{Ma} \gg 1$), the leading-order terms are the ones that

have $\mathrm{Kn}^2\mathrm{Ma}^2$ as the coefficient. It can thus be concluded that for compressible flows, the deviation of τ_{xy} and q_y from the NSF equation scales as $\mathrm{Kn}^2\mathrm{Ma}^2$. The deviation of normal stresses from the NSF equation scales with Kn and Ma independently. When $\mathrm{Kn} \gg \mathrm{Ma}$, the deviation of normal stress from the continuum hypothesis scales according to Kn^2, and when $\mathrm{Kn} \ll \mathrm{Ma}$, it scales as Ma^2, as seen from Eqs. (21) and (22).

Comparison of analytical result with data. We now compare the scalings discussed in the previous section with the computational results of the authors presented in Refs. [11,12]. The work uses the finite-volume-based method with discretization in velocity space for solving the Boltzmann transport equation, known as the unified gas kinetic scheme (UGKS) [32,33]. The method has been extensively validated by the authors [11,34]. A domain of size $L_x \times L_y$ was initialized with a tan hyperbolic velocity profile and a

periodic boundary condition is used in the streamwise direction. In the transverse direction of the mixing layer, a zero gradient boundary condition is used. A schematic of the domain can be found in Mohan *et al.* [12]. The computation examines the development of mixing layers for different Knudsen number based on the vorticity thickness and convective Mach number, given as $Kn = \lambda/\delta$ and $Ma_c = \Delta u/2\sqrt{\gamma RT_\infty}$, respectively. Here, λ is the mean-free path of the medium, δ is the mixing layer thickness, Δu is the difference in speed of the free stream, γ is the ratio of specific heat capacity, and T_∞ is the free-stream temperature of the mixing layer. Computations have been performed, $Ma_c = 0.1$–1.2, with increments of 0.1 in Mach number and the initial Knudsen number, $Kn_0 = \lambda/\delta_{t=0} = 0.01$. Other initial Knudsen numbers of $Kn_0 = 0.1, 0.5$, and 1.0 were also tried. The scalings shown in Nondimensionalization of equations were observed for the lower Kn_0, whereas at higher Kn_0, these scalings were not seen, especially for the higher Mach numbers. This could be because at higher Mach and Knudsen numbers, the Grad 13 moment equations and the approximations (iv) and (v) in Grad 13 moment equations would not be valid. In the computation, the length of the domain is taken as $L_x = 20\delta_0$ and $L_y = 80\delta_0$, where δ_0 is the initial vorticity thickness of the mixing layer. The domain is discretized into $N_x \times N_y = 128 \times 604$ grid points. The velocity space is discretized into $c_x \times c_y = 28 \times 28$ discrete ordinates and the Gauss-Hermite quadrature is used. A detailed discussion on discretization is given in Ref. [11].

The Prandtl number Pr is kept equal to unity and the ratio of specific heat capacity, $\gamma = 1.667$, in the study. Monoatomic gas is considered for the present computation. The temperature is initialized using the Crocco-Busemann relationship, and the pressure is kept constant throughout the field. The densities of both of the free streams are equal. The PDF is initialized using the Maxwellian distribution function. The domain is periodic in the streamwise direction and a zero gradient is used for all the quantities in the transverse direction.

The deviation of the stress and transverse heat flux from the NSF is calculated as follows:

$$\Delta\tau_{xy} = \frac{|\tau_{xy,NS} - \tau_{xy,B}|}{\mu_\infty \Delta u/\delta}, \tag{25}$$

$$\Delta\tau_{xx} = \frac{|\tau_{xx,NS} - \tau_{xx,B}|}{\mu_\infty^2/(\rho_\infty \delta^2)}, \tag{26}$$

$$\Delta\tau_{yy} = \frac{|\tau_{yy,NS} - \tau_{yy,B}|}{\mu_\infty^2/(\rho_\infty \delta^2)}, \tag{27}$$

$$\Delta q_y = \frac{|q_{y,NS} - q_{y,B}|}{\mu_\infty \Delta u^2/\delta}, \tag{28}$$

where μ_∞ is the viscosity of the fluid in the free stream.

Figure 1 shows the peak deviation of shear stress from the NSF equation, $\Delta\tau_{xy}$, against time-varying Knudsen Kn. Red dashed reference lines are included, which show Kn^2 and $(KnMa_c)^2$, and the black arrow indicates increasing convective Mach number in Figs. 1 and 2. As noted earlier in [12], the deviation of shear stress of the low Mach number case collapses on each other when they are scaled with the Knudsen number alone. Likewise, in the high Mach number cases, the
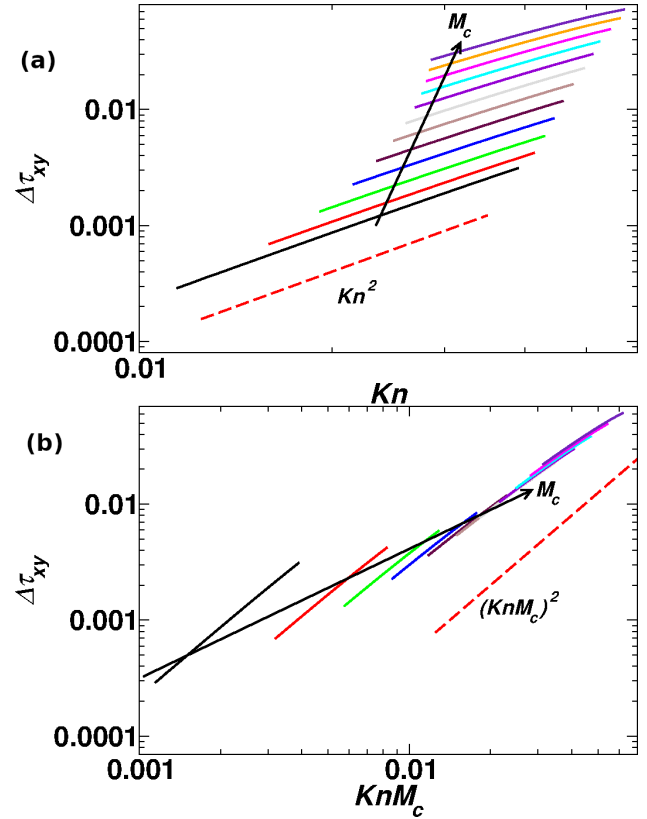

FIG. 1. Scaling of the peak deviation of shear stress, $\Delta\tau_{xy}$, with Knudsen number Kn at various Mach numbers Ma_c. Solid lines are from the present UGKS simulation, and dashed lines are the slope of predictions from the present theory. It can be inferred that (a) when $KnMa_c \ll Kn$ (i.e., when $Ma_c \ll 1$), $\Delta\tau_{xy}$ scales as Kn^2, and (b) when $KnMa_c \gg Kn$ (i.e., when $Ma_c \gg 1$), $\Delta\tau_{xy}$ scales as $(KnMa_c)^2$.

collapse occurs when the deviation of shear stress is scaled with the product of the Knudsen number and Mach number. It can be seen that the low Mach number cases scale with Kn^2, while the high Mach number cases scale well with $(KnMa_c)^2$. A similar analysis is done for q_y, as shown in Fig. 2. The low Mach number curves collapse on each other when Δq_y is plotted against Kn, whereas the high Mach number cases collapse when it is plotted against $KnMa_c$. It is seen that for the low Mach number cases, the deviation of transverse heat flux from the NSF equation scales as Kn^2, whereas at high Mach number cases, the deviation scales as $(KnMa_c)^2$.

Figure 3 shows the scaling of peak deviation of normal stresses, $\Delta\tau_{xx}$ and $\Delta\tau_{yy}$, with convective Mach number at instantaneous $Kn = 0.075$. It can be seen from the figure that both $\Delta\tau_{xx}$ and $\Delta\tau_{yy}$ increase with the increase in Mach number. The black circles in the figure are the values of $\Delta\tau_{xx}$ and $\Delta\tau_{yy}$ obtained from the numerical simulation of mixing layers, whereas the red dotted line shows the scaling of this data with Ma_c. The deviation of τ_{xx} and τ_{yy} scales as Ma_c^2, which is close to the theoretical prediction given in Eqs. (21) and (22).

Conclusion. The work examined the effect of rarefaction and compressibility on the continuum breakdown for temporally developing parallel shear flows. The degree of departure of the stress tensor and the heat-flux components from their
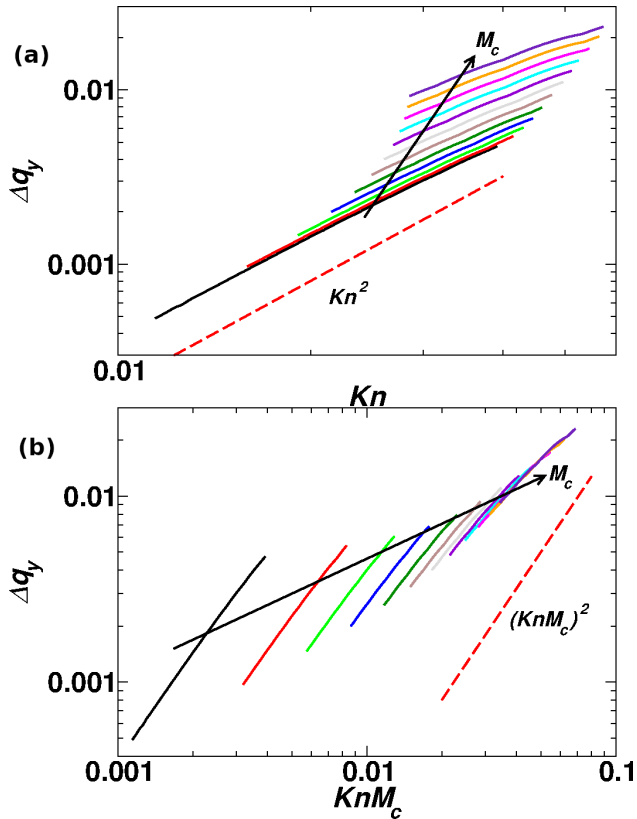
FIG. 2. Scaling of the peak deviation of transverse heat flux, Δq_y, with Knudsen number Kn at various Mach number, Ma_c. Solid lines are from the present UGKS simulation, and dashed lines are the slope of predictions from the present theory. Similar inferences as in Fig. 1 can also be made here.

FIG. 3. Scaling of the peak deviation of normal stresses, $\Delta \tau_{xx}$ and $\Delta \tau_{yy}$, with convective Mach number Ma_c, at Kn = 0.075. The deviation scales as Ma_c^2 as given in Eqs. (21) and (22).

respective NSF values is computed from the UGKS simulation data. The Mach and Knudsen number scaling of the magnitude of departure is compared to Grad 13 model estimates. Mohan *et al.* [13] demonstrate that the Grad 13 model is indeed accurate in the parameter regime $Ma_c \leqslant 1.2$ and $Kn_0 \leqslant 1$. The limitations of Grad 13 for accurately capturing the physics of rarefied flows will be examined in future works. The Grad 13 moment equations were nondimensionalized using continuum thin shear layer scaling. The nondimensional equations showed multiple parameters of importance for the
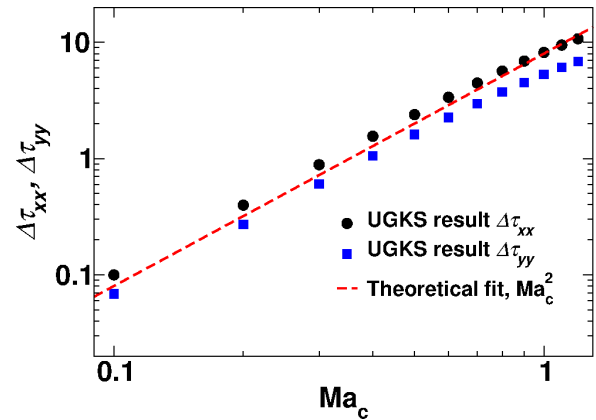
stress and heat-flux components. At specific ranges of Mach number, the contribution of different terms in the stress and heat-flux equations is dominant. Based on this observation, two regimes for deviation from the NSF equation are identified. At low Mach number, the only parameter that determines the deviation from the NSF equation is the Knudsen number. The deviation of all the stress and heat-flux components from the NSF equation in this regime scales according to Kn^2. At high Mach numbers, the parameter that determines the deviation is KnMa. However, this parameter turns out to be important only for two of the nonequilibrium variables, namely, q_y and τ_{xy}. In this regime, the deviation of τ_{xy} and q_y scales as Kn^2Ma^2. It is seen that the deviation of τ_{xx} and τ_{yy} from the NSF equation depends on Kn and Ma, independently, and scales as Kn^2 and Ma^2 depending on the relative magnitude of Kn and Ma. Finally, it is shown that the scaling analysis for the Grad 13 equation is in agreement with the numerical data for mixing layers in a compressible and rarefied medium.

[1] V. Venugopal, D. S. Praturi, and S. S. Girimaji, Non-equilibrium thermal transport and entropy analyses in rarefied cavity flows, J. Fluid Mech. **864**, 995 (2019).

[2] N. Singh and T. E. Schwartzentruber, Heat flux correlation for high-speed flow in the transitional regime, J. Fluid Mech. **792**, 981 (2016).

[3] N. Singh and T. E. Schwartzentruber, Aerothermodynamic correlations for high-speed flow, J. Fluid Mech. **821**, 421 (2017).

[4] Z. Wang, L. Bao, and B. Tong, Rarefaction criterion and non-Fourier heat transfer in hypersonic rarefied flows, Phys. Fluids **22**, 126103 (2010).

[5] P. Bhattacharya, M. P. Manoharan, R. Govindarajan, and R. Narasimha, The critical Reynolds number of a laminar incompressible mixing layer from minimal composite theory, J. Fluid Mech. **565**, 105 (2006).

[6] M. Lessen, J. A. Fox, and H. M. Zien, On the inviscid stability of the laminar mixing of two parallel streams of a compressible fluid, J. Fluid Mech. **23**, 355 (1965).

[7] N. D. Sandham and W. C. Reynolds, Three-dimensional simulations of large eddies in the compressible mixing layer, J. Fluid Mech. **224**, 133 (1991).

[8] A. W. Vreman, N. D. Sandham, and K. H. Luo, Compressible mixing layer growth rate and turbulence characteristics, J. Fluid Mech. **320**, 235 (1996).

[9] C. Pantano and S. Sarkar, A study of compressibility effects in the high-speed turbulent shear layer using direct simulation, J. Fluid Mech. **451**, 329 (2002).

[10] S. Arun, A. Sameen, B. Srinivasan, and S. S. Girimaji, Topology-based characterization of compressibility effects in mixing layers, J. Fluid Mech. **874**, 38 (2019).

[11] V. Mohan, A. Sameen, B. Srinivasan, and S. S. Girimaji, Influence of Knudsen and Mach numbers on Kelvin-Helmholtz instability, Phys. Rev. E **103**, 053104 (2021).

[12] V. Mohan, A. Sameen, B. Srinivasan, and S. S. Girimaji, Continuum breakdown in compressible mixing layers, Phys. Rev. E **105**, 065102 (2022).

[13] H.-S. Tsien, Superaerodynamics, mechanics of rarefied gases, J. Aeronaut. Sci. **13**, 653 (1946).

[14] G. A. Bird, Breakdown of translational and rotational equilibrium in gaseous expansions, AIAA J. **8**, 1998 (1970).

[15] I. D. Boyd, G. Chen, and G. V. Candler, Predicting failure of the continuum fluid equations in transitional hypersonic flows, Phys. Fluids **7**, 210 (1995).

[16] C. Schrock, R. McMullan, and J. Camberos, Continuum onset parameter based on entropy gradients using Boltzmann's H-theorem, in *Proceedings of the 43rd AIAA Aerospace Sciences Meeting and Exhibit* (AIAA, Reno, Nevada, 2005).

[17] C. Schrock, R. McMullan, and J. Camberos, Calculation of entropy generation rates via DSMC with application to continuum/equilibrium onset, in *Proceedings of the 38th AIAA Thermophysics Conference* (AIAA, Toronto, Ontario, 2005).

[18] D. A. Lockerby, J. M. Reese, and H. Struchtrup, Switching criteria for hybrid rarefied gas flow solvers, Proc. R. Soc. A: Math. Phys. Eng. Sci. **465**, 1581 (2009).

[19] S. Chigullapalli, A. Venkattraman, M. S. Ivanov, and A. A. Alexeenko, Entropy considerations in numerical simulations of non-equilibrium rarefied flows, J. Comput. Phys. **229**, 2139 (2010).

[20] J. Meng, N. Dongari, J. M. Reese, and Y. Zhang, Breakdown parameter for kinetic modeling of multiscale gas flows, Phys. Rev. E **89**, 063305 (2014).

[21] A. Alamatsaz and A. Venkattraman, Characterizing deviation from equilibrium in direct simulation Monte Carlo simulations, Phys. Fluids **31**, 042005 (2019).

[22] S. Tiwari, Coupling of the Boltzmann and Euler equations with automatic domain decomposition, J. Comput. Phys. **144**, 710 (1998).

[23] J. Ou and J. Chen, Nonlinear transport of rarefied Couette flows from low speed to high speed, Phys. Fluids **32**, 112021 (2020).

[24] M. Macrossan, Scaling parameters for hypersonic flow: Correlation of sphere drag data, in *Proceedings of the 25th International Symposium on Rarefied Gas Dynamics*, edited by M. S. Ivanov and A. K. Rebrov (Siberian Branch of the Russian Academy of Sciences, St. Petersburgh, 2007), Vol. 1, pp. 759–764.

[25] W. Weiss, Continuous shock structure in extended thermodynamics, Phys. Rev. E **52**, R5760(R) (1995).

[26] H. Struchtrup, *Macroscopic Transport Equations for Rarefied Gas Flows: Approximation Methods in Kinetic Theory* (Springer, Berlin, 2005).

[27] H. Grad, On the kinetic theory of rarefied gases, Commun. Pure Appl. Math. **2**, 331 (1949).

[28] H. Struchtrup, Stable transport equations for rarefied gases at high orders in the Knudsen number, Phys. Fluids **16**, 3921 (2004).

[29] H. Struchtrup, Derivation of 13 moment equations for rarefied gas flow to second order accuracy for arbitrary interaction potentials, Multiscale Model. Simulat. **3**, 221 (2005).

[30] W. G. Vincenti and C. H. Kruger, *Introduction to Physical Gas Dynamics* (Krieger, Malabar, Florida, 1965).

[31] F. M. White, *Viscous Fluid Flow* (McGraw Hill, New York, 2006).

[32] K. Xu and J.-C. Huang, A unified gas-kinetic scheme for continuum and rarefied flows, J. Comput. Phys. **229**, 7747 (2010).

[33] J.-C. Huang, K. Xu, and P. Yu, A unified gas-kinetic scheme for continuum and rarefied flows II: Multi-dimensional cases, Commun. Comput. Phys. **12**, 662 (2012).

[34] V. Venugopal and S. S. Girimaji, Unified gas kinetic scheme and direct simulation Monte Carlo computations of high-speed lid-driven microcavity flows, Commun. Comput. Phys. **17**, 1127 (2015).